

# Primordial black holes and secondary gravitational waves from the inflation potential with a tiny Lorentz function bump

Wei Yang<sup>a\*</sup>, Yu-Xuan Kang<sup>b†</sup>, Arshad Ali<sup>c‡</sup>, Tao-Tao Sui<sup>a§</sup>, Chen-Hao Wu<sup>a¶</sup>, and Ya-Peng Hu<sup>a,d\*\*</sup>

<sup>a</sup>College of Physics, Nanjing University of Aeronautics and Astronautics, Nanjing, 211106, China

<sup>b</sup>School of Physics Sciences, University of Science and Technology of China, Hefei 230026, China

<sup>c</sup>Institute for Advanced Study & School of Physical Science and Technology,

Soochow University, Suzhou 215006, P.R. China

<sup>d</sup>Key Laboratory of Aerospace Information Materials and Physics (NUAA), MIIT, Nanjing 211106, China

This paper explores the generation of primordial black holes (PBHs) and scalar-induced gravitational waves (SIGWs) from the inflation potential with a tiny Lorentz function bump. We choose the Starobinsky model as basic potential, which satisfies the condition of observational constraints of the CMB at a large scale. We find that the tiny Lorentz function bump can enhance the primordial curvature power spectrum to  $\mathcal{O}(10^{-2})$  at a small scale, leading to the formation of PBHs with sufficient abundance. Furthermore, we discover that the abundance of PBHs with mass  $10^{-12}M_{\odot}$  is approximately 1, which can make up almost all dark matter. In addition, the SIGWs generated by our models can be tested by the Square Kilometre Array (SKA), Pulsar Timing Arrays (PTA), TianQin, Taiji, Laser Interferometer Space Antenna (LISA), and DECIGO. It should be emphasized that, compared with the tiny Gaussian bump case, the Lorentz function bump case can easily produce a sufficient abundance of PBHs with a wider mass range, and accompanying a broader frequency range of SIGWs, which predicts the advantage of the Lorentz function bump for basic potential with big e-folding number  $N$  around  $55 \sim 60$ .

PACS numbers:

## I. INTRODUCTION

The investigation of gravitational waves (GWs) has played a pivotal role in cosmology and astrophysics since the formulation of the theory of general relativity in the 20th century. The Laser Interferometer Gravitational-Wave Observatory (LIGO) achieved a historic milestone by successfully detecting GW signals originating from binary black hole mergers [1]. Subsequently, the LIGO/Virgo collaborations extended this achievement to encompass mergers involving black holes and neutron stars, ushering in a new era of multi-messenger astronomy [2]. Notably, the emergence of GW signals from such events has spurred heightened interest in primordial black holes (PBHs) as they are posited to explain binary black hole mergers [3, 4].

Several astrophysical observations provide credible evidence that dark matter (DM) is the non-negligible element of our universe [5–8]. As viable candidates of cold DM, PBHs have also attracted lots of attention [9–17]. A large number of different types of cosmological and astronomical observations have been made on the abundance of primordial black holes as dark matter in many mass ranges limit is given [18–25]. However, the abundances of PBHs at the mass windows of  $10^{-17} - 10^{-15}M_{\odot}$  and

$10^{-14} - 10^{-12}M_{\odot}$  are largely unconstrained by observations and specific assumptions, and can make up almost all of the DM [26], and PBHs with planetary masses can explain the ultrashort-timescale microlensing events in the OGLE data [27, 28].

There are many PBH formation mechanisms, the most popular one is the overdense region gravitational collapse inside a Hubble horizon, where the density exceeds the threshold value [29]. Many situations can form the overdense region, such as enhancement of curvature perturbation [30–43], accumulation of topological defect [44–47], and postponed false vacuum decay during first-order transition [48, 49]. Beyond PBHs, these perturbations also contribute to the production of scalar-induced gravitational waves (SIGWs) [50–60], which can be tested by the North American Nanohertz Observatory for Gravitational Wave (NANOGrav) [61], Pulsar Timing Arrays (PTA) [62, 63] and space-based GW detectors, such as the Laser Interferometer Space Antenna (LISA) [64], Taiji [65], TianQin [66], and Deci-hertz Interferometer Gravitational-Wave Observatory (DECIGO) [67] in the future. We need a sufficient large-density perturbation at a small scale to produce a sufficient abundance of PBHs as DM and detectable SIGWs.

Recently, constructing a local bump form on the basic inflation potential function is a common mechanism that single-field inflation generates PBHs [68–71]. Due to the addition of the local bump form, the bump usually contributes an additional  $\Delta N$  on the basis of the inflation e-folding  $N_b$  provided by the basic potential function. In the previous work, the basic potential function is usually selected with  $N_b \sim 45$ , and one can adopt the bumps with the Gaussian function or Hyperbolic function to generate

\*yw1214@nuaa.edu.cn

†yxkang@mail.ustc.edu.cn

‡arshadali@suda.edu.cn

§taotaosui@nuaa.edu.cn

¶chenhao\_wu@nuaa.edu.cn

\*\*huyp@nuaa.edu.cn, corresponding author

the PBHs with various mass ranges [71]. Note that, one typically needs a quasi-de-sitter inflationary period lasting for at least 60 – 70 e-folding of expansion [71]. If the basic inflation potential has a big e-folding number  $N$  around 55 ~ 60, the  $\Delta N$  will be restricted, which may reflect on the choice of bump function. Therefore, it is interesting to investigate the effect of different bump function forms on that basic inflation potential. In our paper, we choose the Starobinsky model as the basic inflation potential, whose e-folding number is very large with  $N_b \sim 59$ . We discover that the Gaussian function or Hyperbolic function cases do not produce sufficient abundance for the PBHs with stellar mass, while the Lorentz function bump case can, which predicts the advantage of the Lorentz function bump for the basic inflation potential with large e-folding number  $N$ .

This paper is organized as follows. In section II, we calculate the slow-roll parameters for the two bump forms. In section III, we numerically calculate the power spectrum of the primordial curvature perturbations,  $n_s$ ,  $r$ , and the abundance of PBH for models. In section IV, we study the energy density spectrum of SIGWs for models. Finally, we draw our conclusion and discussion in section V.

## II. SLOW-ROLL INFLATION AND A TINY BUMP IN POTENTIAL

### A. Slow-roll inflation

In this paper, we study single-field inflation, and its corresponding action is

$$S = \int d^4x \sqrt{-g} \left[ \frac{1}{2}R - \frac{1}{2}g_{\mu\nu} \nabla^\mu \phi \nabla^\nu \phi - V(\phi) \right]. \quad (1)$$

In the context of a spatially flat homogeneous and isotropic universe with FLRW metric  $ds^2 = -dt^2 + a(t)\delta_{ij}dx^i dx^j$ , the Friedmann equation and dynamical equations of the inflation field  $\phi$  are as follows [31]

$$\begin{aligned} 3H^2 &= \frac{1}{2}\dot{\phi}^2 + V(\phi), \\ \dot{H} &= -\frac{1}{2}\dot{\phi}^2, \\ \ddot{\phi} + 3H\dot{\phi} + V_\phi(\phi) &= 0. \end{aligned} \quad (2)$$

Here,  $a(t)$  is the scale factor, and  $H = \dot{a}/a$  represents the Hubble parameter. For the homogeneous background, the inflation field is only time-dependent, i.e.,  $\phi = \phi(t)$ .

During the inflation epoch, the scalar field's movement is characterized by extreme slowness, with the potential energy being the dominant contributor to the scalar field's energy. The scalar field adheres to the slow-roll condition, which entails  $\frac{1}{2}\dot{\phi}^2 \ll V(\phi)$  and  $|\ddot{\phi}| \ll 3H|\dot{\phi}|$ . The dynamic equations could be written approximately as [32, 37]

$$3H^2 \simeq V(\phi), \quad 3H\dot{\phi} \simeq -V_\phi(\phi). \quad (3)$$

The slow-roll parameters are defined as

$$\epsilon_H = -\frac{\dot{H}}{H^2}, \quad \eta_H = -\frac{\ddot{\phi}}{H\dot{\phi}}. \quad (4)$$

The  $\epsilon_H \ll 1$ ,  $|\eta_H| \ll 1$  during inflation, the end of inflation condition is  $\epsilon_H = 1$ .

It is not difficult to see that the potential function changes slightly near  $\phi_0$ , leading to the number of e-folding being superimposed during inflation. According to the formula of the number of e-folding

$$N = \int_{\phi_{in}}^{\phi_*} \frac{1}{\sqrt{2\epsilon_H}} d\phi, \quad (5)$$

where  $\phi_{in}$  is scalar field parameter in inflation.

The well-known slow-roll approximation formula for the power spectrum of primordial scalar perturbation is given by [31, 32]

$$P_\zeta = \frac{H^2}{8\pi^2\epsilon_H}. \quad (6)$$

It is inversely proportional to the slow-roll parameter  $\epsilon_H$ , and due to the flattening of the potential energy near  $\phi_0$ , the Hubble parameter  $H$  can be approximated as constant from Eq. (3). Therefore, we can approximate the magnitude of the power spectrum according to  $\epsilon_H$ .

### B. A tiny bump in potential

In this paper, our model of a small local perturbation forming PBH is a basic potential with the general form [71]

$$V(\phi) = V_b(1 + f(\phi)). \quad (7)$$

We here consider this general form of the potential as a phenomenological model. Where  $V_b$  is the basic inflation potential responsible for generating quantum fluctuations compatible with the CMB constraints. Here  $f(\phi)$  represents a tiny local bump whose value is much smaller than 1.

Of the numerous inflation models, the Starobinsky inflation model is almost the most well-known one and it is well-aligned with current CMB measurements [72, 73]. We choose the basic potential  $V_b$  in Eq. (7) is associated with this inflation model

$$V_b = \frac{3}{4}m^2 \left(1 - e^{-\sqrt{\frac{2}{3}}\phi}\right)^2, \quad (8)$$

where  $m = 1.13 \times 10^{-5}m_p$  denotes the mass parameter. Here, we adopt the reduced Planck mass as  $m_p = \frac{1}{\sqrt{8\pi G}} = 1$ .

We introduce a Lorentz function form of this local bump as

$$f_L(\phi) = \frac{b}{1 + \left(\frac{\phi - \phi_0}{c}\right)^2}, \quad (9)$$

the Lorentz function acts as a local bump in the potential function, and the  $c$  and  $\phi_0$  control the width and the bump position of the potential function, respectively.  $\phi_0$  is also a field value in inflation, and  $b$  represents the amplitude, and the nature of the small perturbations causes  $b$  to be limited to a range of  $0 < b \ll 1$ . Notably, when  $b = 0$ , the model reduces to the Starobinsky inflation model for the Eq. (7). For this Starobinsky inflation model with Lorentz function bump is written as

$$V_L(\phi) = \frac{3}{4}m^2 \left(1 - e^{-\sqrt{\frac{2}{3}}\phi}\right)^2 \left(1 + \frac{b}{1 + \left(\frac{\phi - \phi_0}{c}\right)^2}\right). \quad (10)$$

In this paper, we choose the initial value time of inflation  $\phi_* = 5.42$ , which makes  $\epsilon_H(\phi_*) \approx 10^{-4}$  satisfies the slow-roll condition, and we can obtain  $\phi_{\text{end}} = 0.614$  by  $\epsilon_H(\phi_{\text{end}}) = 1$ . Therefore, the parameter  $\phi_0$  of the bump function has a range value of  $0.614 < \phi_0 < 5.42$ . According to the above constraints of  $b$  and  $c$ , we choose an optimal set of parameters,  $b = 4 \times 10^{-4}$ ,  $c = 0.00999311$ ,  $\phi_0 = 5.1$ , and they are brought into Eq. (9) to satisfy  $f_L(\phi) \ll 1$ . The evolution of the potential function containing a bump for  $\phi$  is shown in Fig. 1.

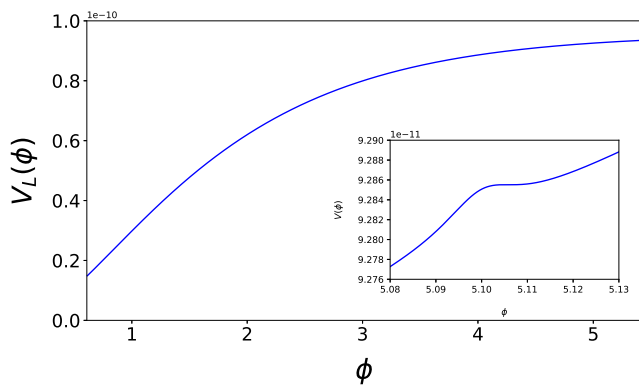


FIG. 1: The evolution of the potential function containing a Lorentz bump for  $\phi$  at  $b = 0.0004$ ,  $c = 0.00999311$ ,  $\phi_0 = 5.1$ .

It should be pointed out that, for the above basic Starobinsky potential function, whose e-folding number  $N_b$  is 59, the upper limit of  $\Delta N$  due to local bump is 11 in our paper. In Fig. 2(a)<sup>1</sup>, we have presented the relationship between the e-folding number  $N$  and inflation single scalar field  $\phi$  after considering the Lorentz bump function.

<sup>1</sup> Here and after, we use the blue real line to present the investigations on the tiny bump with the Lorentz function case. Note that, in previous work, one often takes the bump with the Gaussian function into account. In fact, we have also investigated the Gaussian function case later. However, to compare with the Gaussian function case explicitly, we have added the results of the Gaussian function case in the same figure, i.e., distinguishing by using the red dashed line.

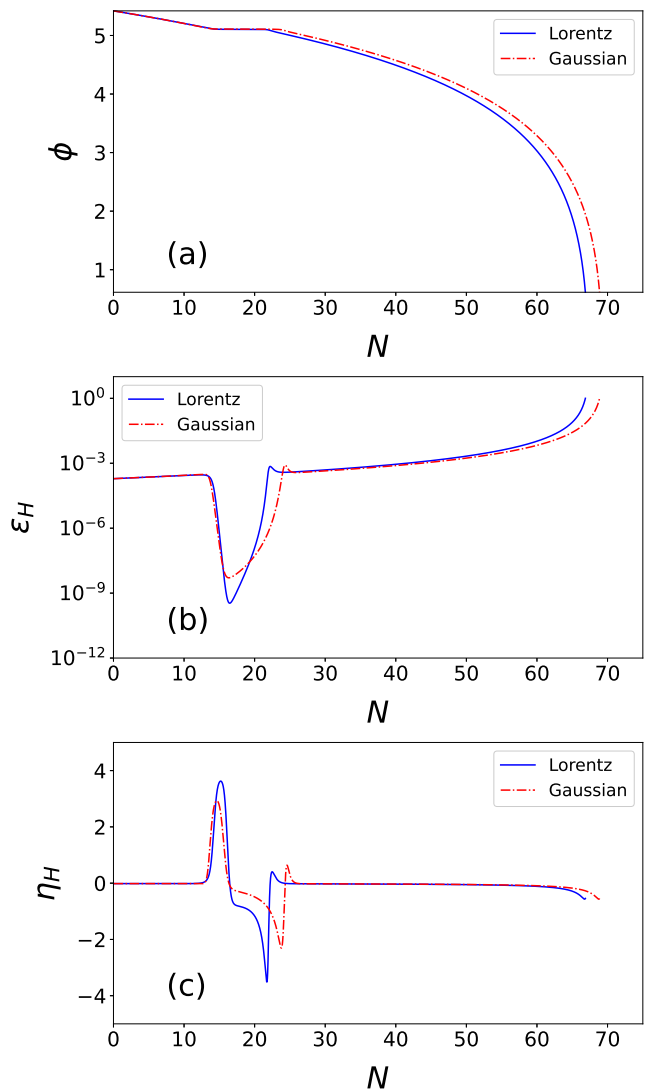


FIG. 2: (a) shows the evolutions of e-folds number  $N$ . (b) shows the evolutions of the first slow-roll parameter  $\epsilon_H$ . (c) shows the evolutions of the second slow-roll parameter  $\eta_H$ . We represent Gaussian and Lorentz with red dotted lines and blue solid lines, respectively, where the parameter selection is  $b = 0.0004$ ,  $c = 0.00999311$ ,  $\phi_0 = 5.1$ .

From this figure, we can find that the above parameters  $b, c, \phi_0$  indeed satisfy the inflation constraint  $N \leq 70$ , i.e., the  $\phi$  closer to  $\phi_{\text{end}}$  can keep the total number of e-folding  $N \sim 67$  and the extra e-folding number  $\Delta N \approx 8$  near the  $\phi_0 \approx 5.1$ . Moreover, we find the slow-roll parameter  $\epsilon_H \ll 1$  during inflation and  $\epsilon_{H\text{min}} \sim 10^{-10}$ , signifying a reduction of six orders of magnitude compared to the initial value of  $\epsilon_H(\phi_*) \sim 10^{-4}$  from the solid line in Fig. 2(b). Therefore, we obtain the approximate power spectrum is  $\mathcal{O}(10^{-3})$  from Eq. (6). The requirements for generating PBHs with sufficient abundance cannot be met.

Above we analyze the results of the slow-roll approximation of the Lorentz function bump. Next, we will study

the Gaussian function to compare it with the Lorentz function. The Gaussian bump is written as [71]

$$f_G(\phi) = be^{-\frac{(\phi-\phi_0)^2}{2c^2}}, \quad (11)$$

these parameters  $b, c, \phi_0$  control the amplitude, width, and center position of the bump, respectively. We use the subscript L and G hereinafter to represent Lorentz and Gaussian, respectively.

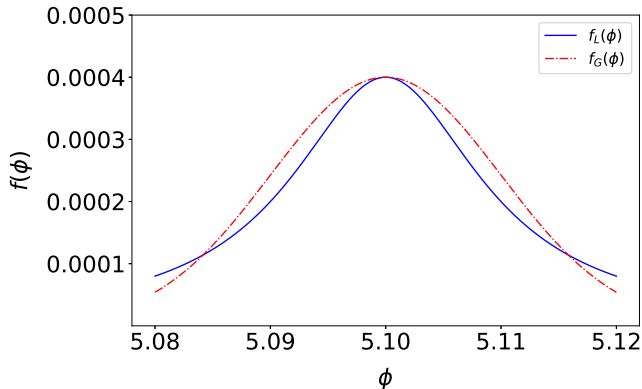


FIG. 3: Gaussian function versus Lorentz function. We represent the Gaussian function and Lorentz function with red dotted lines and blue solid lines, respectively, where the parameter selection is  $b = 0.0004, c = 0.00999311, \phi_0 = 5.1$ .

Firstly, for the Gaussian case, we choose the same parameters of the Lorentz function and compare the two bump forms as shown in Fig. 3. From the figure, it is not difficult to see that the Lorentz function shows a narrower peak width near the  $\phi_0 = 5.1$ . This phenomenon might imply the flat length of Lorentz potential appears slightly shorter near  $\phi_0 = 5.1$  compared to the Gaussian potential. This Starobinsky inflation model with Gaussian bump is written as

$$V_G(\phi) = \frac{3}{4}m^2 \left(1 - e^{-\sqrt{\frac{2}{3}}\phi}\right)^2 \left(1 + be^{-\frac{(\phi-\phi_0)^2}{2c^2}}\right). \quad (12)$$

We also choose the initial value time of inflation  $\phi_* = 5.42$ . For the Gaussian case, We plot the evolution of potential as shown in Fig. 4, the flat length in the Lorentz case is indeed shorter. Moreover, in Fig. 2(a), we can find that the total number of e-folding  $N \approx 69$  before the inflation end, and the  $\Delta N \approx 10$  generated by a bump. Then, due to the slow-roll parameter  $\epsilon_{H\min} \approx 10^{-9}$  of Gaussian bump in Fig. 2(b), and the power spectrum can be approximated to  $\mathcal{O}(10^{-4})$  according to Eq. (6).

Through further comparative analysis, we find that the narrow peak value of the Lorentz function leads to the narrow flatness of potential at  $\phi_0$  and may lead to the additional contribution  $\Delta N$  value is relatively small, and the power spectrum enhanced by the Lorentz bump is larger than that of the Gaussian bump under the same parameters. Thus the Lorentz bump is easier to satisfy the inflationary constraint and shows more advantages than the Gaussian case.

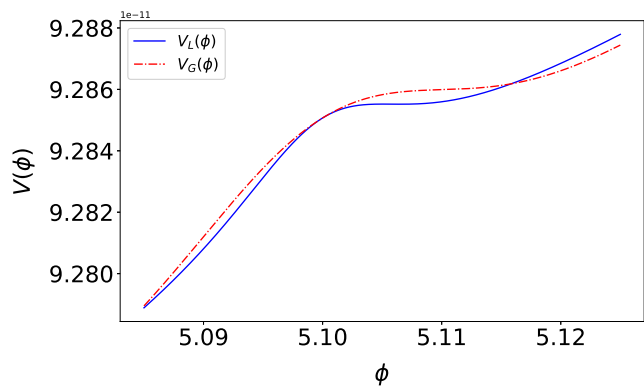


FIG. 4: The evolution of the potential functions with Gaussian bump (red dotted lines) and Lorentz bump (blue solid lines), and the parameter selection is  $b = 0.0004, c = 0.00999311, \phi_0 = 5.1$ .

In addition, when entering an ultra-slow roll period, the  $\epsilon_H \ll 1$  implies inflation does not end. However, the  $|\eta_H|$  greater than 1 for a short period seems to violate the slow roll condition as shown in Fig. 2(c). Therefore, Eq. (6) cannot be used to calculate the power spectrum [32, 37, 74], we will calculate the power spectrum numerically to make an accurate comparison in the next section.

### III. THE POWER SPECTRUM AND PRIMORDIAL BLACK HOLE

In this section, we first investigate the behavior of the power spectrum for primordial curvature perturbation to ensure it satisfies the constraints of cosmic microwave background (CMB) observations. By numerically solving the Mukhanov-Sasaki equation [75, 76]

$$\frac{d^2 v_k}{d\eta^2} + \left(k^2 - \frac{1}{z} \frac{d^2 z}{d\eta^2}\right) v_k = 0, \quad (13)$$

where the conformal time  $d\eta = dt/a$ , the quantum canonical field  $v_k = z\zeta_k$  and  $z = a\dot{\phi}/H$ , we can obtain the scalar power spectrum

$$P_\zeta = \frac{k^3}{2\pi^2} \frac{|v_k|^2}{z^2}. \quad (14)$$

First, we try to calculate the power spectrum numerically and compare the power spectrum generated by the Lorentz bump and Gaussian bump with the same parameters  $b = 4 \times 10^{-4}, c = 0.00999311, \phi_0 = 5.1$ . We can see that the power spectrum of the Lorentz function can reach  $\mathcal{O}(10^{-2})$  as shown by LI in Fig. 5, while the power spectrum of the Gaussian function is  $\mathcal{O}(10^{-4})$  as shown by G in Fig. 5. If we want to enhance the power spectrum to  $\mathcal{O}(10^{-2})$  for Gaussian function bump, then we choose the parameters  $b = 0.000421$  and  $c = 0.0099733$  at  $\phi_0 = 5.1$ . However, it is worth noting that under the set of

parameters, the total e-folding number  $N \sim 79$  before the end of inflation does not meet the constraints of inflation. Therefore, the maximum value of the power spectrum under the inflation constraint ( $N \leq 70$ ) is  $\mathcal{O}(10^{-4})$  as shown by GI in Fig. 5, other data are recorded in Table I. The above numerical analysis shows that while meeting the power spectrum requirements, the Lorentz function bump contributes a smaller value of  $\Delta N$  than the Gaussian function bump, which makes it easier to meet the constraints of inflation.

We also choose a couple of suitable parameters to record for both bump forms, just shown in Table I. Then we numerically calculate the power spectrum. These sets of parameters can not only eliminate the contingency of the single set of parameters model but also broaden the peak scale  $k_{peak}$  range corresponding to the peak of the power spectrum  $P_{peak}$ . In Fig. 5, we find the peak values of the power spectrum can reach the order of  $\mathcal{O}(10^{-2})$  at the scales  $k_{peak} \sim 10^5 Mpc^{-1}$ ,  $k_{peak} \sim 10^8 Mpc^{-1}$  and  $k_{peak} \sim 10^{12} Mpc^{-1}$  for the Lorentz function form as shown LI, LII, and LIII in Table I. However, for the Gaussian bump, only GII and GIII enhance the power spectrum to  $\mathcal{O}(10^{-2})$ , so the Lorentz function corresponds to a wider  $k$  scale.

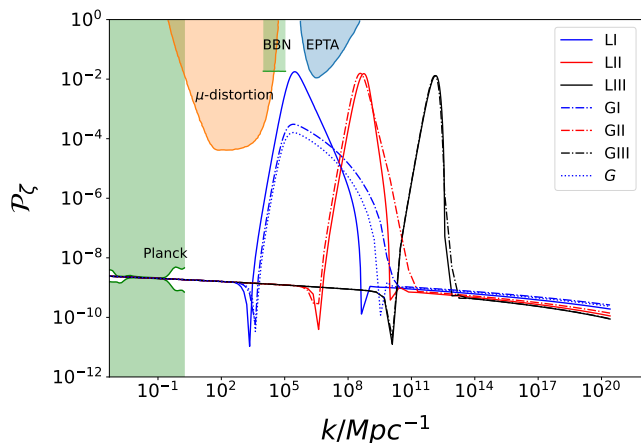


FIG. 5: The scalar power spectrums in the model. The dashed line represents the power spectrum, and the shaded regions represent the observation constraint [77–82].

The local bump of the potential function causes the power spectrum to be enhanced, and the effect on large-scale CMB is discussed below. The Planck 2018 CMB observation provides constraints at a pivot scale of  $k = 0.05 Mpc^{-1}$  and the scalar power spectrum  $A_s = 2.1 \times 10^{-9}$ , such as the scalar spectral index  $n_s = 0.9649 \pm 0.0042 (68\%CL)$  [77, 83] and the latest limitation tensor-to-scalar ratio  $r_{0.05} < 0.036$  of BICEP/Keck 2018 data at 95%CL [84]. The relevant CMB parameters,  $n_s$  and  $r$

are [37]

$$\begin{aligned} n_s &= 1 + \frac{d \ln P_\zeta}{d \ln k} \simeq 1 + 2\eta_H - 4\epsilon_H, \\ r &= \frac{P_T}{P_\zeta} \simeq 16\epsilon_H. \end{aligned} \quad (15)$$

We numerically calculate the scalar spectral index  $n_s$  and the tensor-to-scalar ratio  $r$  as shown in Table I. It is not difficult to see that all sets satisfy the constraints of the observed values. The significance and richness of the primordial curvature perturbation power spectrum peak results indicate that the dark matter abundance of primordial black holes should have corresponding significant results.

Next, we explore the abundance of PBHs within the context of the model. PBHs could form due to the amplification of small-scale curvature perturbations during the inflation process, and they can emerge if the density perturbations exceed a certain threshold. In our paper, the comoving curvature perturbation is assumed to follow the Gaussian distribution. The most simple method to estimate  $\beta$  is to use the Press-Schechter formalism, the fractional energy density of PBHs of the universe is [32, 85]

$$\beta = \frac{\rho_{PBH}}{\rho_{tot}} \approx \text{erfc} \left( \frac{9\delta_c}{4\sqrt{2}P_\zeta} \right) \approx \sqrt{\frac{2}{\pi}} \frac{\sqrt{P_\zeta}}{\mu_c} e^{-\frac{\mu_c^2}{2P_\zeta}}, \quad (16)$$

where  $\rho_{tot}$  and  $\rho_{PBH}$  represent the energy density of the cosmic background and PBHs, respectively. The  $\text{erfc}(x)$  is the complementary error function and  $\mu_c = 9\delta_c/4$  in the radiation-dominated period [32]. The threshold of density perturbation for the formation of the PBHs can be  $\delta_c = 0.4$  [86].

The PBHs abundance is given as [14, 32]

$$\begin{aligned} Y_{PBH} &= \frac{\beta}{3.94 \times 10^{-9}} \left( \frac{\gamma}{0.2} \right)^{\frac{1}{2}} \left( \frac{g_*}{10.75} \right)^{-\frac{1}{4}} \\ &\times \left( \frac{0.12}{\Omega_{DM} h^2} \right) \left( \frac{M_{PBH}}{M_\odot} \right)^{-\frac{1}{2}}. \end{aligned} \quad (17)$$

In this equation, the numerical factor  $\gamma = 0.2$ , the effective degrees of freedom  $g_* = 107.5$  for  $T > 300$  GeV and  $g_* = 10.75$  for  $0.5 \text{ MeV} < T < 300$  GeV [87]. The Planck measurements provide the following value for the dark matter abundance  $\Omega_{DM} h^2 = 0.12$  [88],  $h = H/100 = 0.6727 \text{ km} \cdot \text{s}^{-1} \cdot \text{Mpc}^{-1}$ , which measures the Hubble rate in units of 100, and  $M_{PBH}$  and  $M_\odot$  are the mass of PBHs and solar mass, respectively.

The relationship between mass and scale of PBHs is given by

$$M_{PBH} = 3.68 \left( \frac{\gamma}{0.2} \right) \left( \frac{g_*}{10.75} \right)^{-\frac{1}{6}} \left( \frac{k}{10^6 Mpc^{-1}} \right)^{-2} M_\odot. \quad (18)$$

TABLE I: Model parameters and the numerical results

set	$b(10^{-4})$	$c$	$\phi_0$	N	$n_s$	r	$k_{peak}/\text{Mpc}^{-1}$	$P_{\zeta(peak)}$	$\frac{M_{peak}}{M_{\odot}}$	$Y_{PBH}^{peak}$	$f_c/\text{Hz}$
LI	4	0.00999311	5.1	67	0.9679	0.003	$3.13 \times 10^5$	0.018	37.51	0.00059	$4.84 \times 10^{-10}$
LII	4.1	0.00770966	4.89	62	0.9679	0.003	$5.57 \times 10^8$	0.015	$1.186 \times 10^{-5}$	0.026	$8.61 \times 10^{-7}$
LIII	4.4	0.00541278	4.63	61	0.9679	0.003	$3.5 \times 10^{12}$	0.013	$1.83 \times 10^{-12}$	0.862	$2.19 \times 10^{-3}$
GI	4.21	0.00999	5.1	70	0.9678	0.003	$2.49 \times 10^5$	0.0003	59.3	0	$3.9 \times 10^{-10}$
GII	4.13	0.0077345	4.89	64	0.9678	0.003	$3.85 \times 10^8$	0.016	$2.48 \times 10^{-5}$	0.032	$6.4 \times 10^{-7}$
GIII	4	0.0044063	4.63	61	0.9678	0.003	$1.28 \times 10^{12}$	0.013	$2.24 \times 10^{-12}$	0.65	$2.2 \times 10^{-3}$

Combine the numerical results of the power spectrum and Eq. (16) and Eq. (18), we can obtain the peak mass of PBHs, as shown in Fig. 6 and Table I.

We find that the sets of parameters chosen above make the peak scale  $k_{peak}$  cover more ground and have the wider mass range of the PBHs. In other words, PBHs with different masses correspond to different peak scales  $k_{peak}$ , which will give our results a wider scope of application to explain the PBHs theory. Specifically speaking, for set LI, PBHs with the stellar mass of approximately  $30M_{\odot}$  can be generated. Note that the power spectrum peak is small for set GI, so the PBH abundance corresponding to the stellar mass is almost 0, which is not shown in Fig. 6. These PBHs might be explained as the LIGO events [3, 4]. For sets LII and GII, our models produce PBHs with the mass  $M_{PBH} \sim 10^{-5}M_{\odot}$ , which can explain OGLE ultrashort-timescale microlensing events[27, 28] and the anomalous orbits of trans-Neptunian objects [89]. For sets LIII and GIII, PBHs with masses around  $10^{-13} - 10^{-11}M_{\odot}$  make up almost all DM, and the peak abundance is approximate  $Y_{PBH} \approx 1$ . To sum up, we find that the Lorentz bump presents more advantages for producing stellar mass PBH with sufficient abundance.

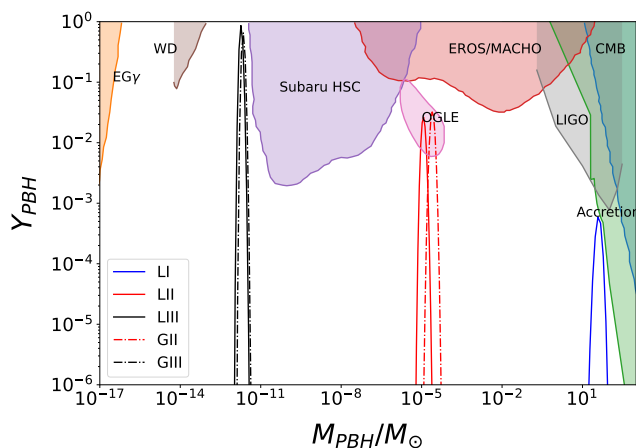


FIG. 6: The abundances of PBHs produced by the model. The dashed line represents the PBH abundance, and the shaded regions represent the constraints on PBHs from various observations[15, 18–25, 27].

#### IV. SCALAR-INDUCED GRAVITATIONAL WAVES

In this section, to investigate the energy density of SIGWs, we shed light on the production of SIGWs. The primordial scalar perturbation starts to evolve after re-entering the event horizon, and its transverse traceless component induces a stochastic gravitational wave background that can be observed by different detectors when the small-scale density perturbation is large enough. Here, we consider the perturbed metric in Newtonian gauge in the cosmological background, which reads [90]

$$ds^2 = -a^2(\eta)(1 + 2\Phi)d\eta^2 + a^2(\eta) \left[ (1 - 2\Phi)\delta_{ij} + \frac{1}{2}h_{ij} \right] dx^i dx^j, \quad (19)$$

where  $a(\eta)$  is the scale factor of the universe. The scalar perturbation  $\Phi$  is of the first order, and the transverse traceless part  $h_{ij}$  is the second-order tensor mode. In the following, we briefly analyze the well-known results on  $h_{ij}$  in the evaluations of SIGWs. The Fourier component equation of  $h_{ij}$  can be expressed as

$$h_{ij}(\eta, \mathbf{x}) = \int \frac{d^3k}{(2\pi)^{3/2}} [e_{ij}^+(\mathbf{k})h_{\mathbf{k}}^+(\eta) + e_{ij}^\times(\mathbf{k})h_{\mathbf{k}}^\times(\eta)] e^{i\mathbf{k}\cdot\mathbf{x}}, \quad (20)$$

where the polarization tensors are defined as [37, 90]

$$e_{ij}^+(\mathbf{k}) = \frac{1}{\sqrt{2}} [e_i(\mathbf{k})e_j(\mathbf{k}) - \bar{e}_i(\mathbf{k})\bar{e}_j(\mathbf{k})], \quad (21)$$

$$e_{ij}^\times(\mathbf{k}) = \frac{1}{\sqrt{2}} [e_i(\mathbf{k})\bar{e}_j(\mathbf{k}) + \bar{e}_i(\mathbf{k})e_j(\mathbf{k})], \quad (22)$$

with  $e_i(\mathbf{k})$  and  $\bar{e}_i(\mathbf{k})$  being normalized vectors orthogonal to each other and to  $k$ . Satisfying  $e_i(\mathbf{k}) \cdot \bar{e}_i(\mathbf{k}) = e_i(\mathbf{k}) \cdot \mathbf{k} = \bar{e}_i(\mathbf{k}) \cdot \mathbf{k}$ . From perturbation of the Einstein's field equations  $G_{\mu\nu} = 8\pi G T_{\mu\nu}$  to the second order, the Fourier component equation of the second order tensor perturbation  $h_k$  is [90–92]

$$h_{\mathbf{k}}''(\eta) + 2\mathcal{H}h_{\mathbf{k}}'(\eta) + k^2h_{\mathbf{k}}(\eta) = 4S_{\mathbf{k}}(\eta), \quad (23)$$

where, ' denotes  $\frac{d}{d\eta}$ ,  $\eta$  is conformal time  $\eta = \int dt/a(t)$ , and the conformal Hubble parameter is  $\mathcal{H} = a'/a$ , and

the source term is [90]

$$S_{\mathbf{k}} = \int \frac{d^3q}{(2\pi)^{3/2}} e_{ij}(\mathbf{k}) q_i q_j \left[ 2\Phi_{\mathbf{q}} \Phi_{\mathbf{k}-\mathbf{q}} + (\mathcal{H}^{-1} \Phi'_{\mathbf{q}} + \Phi_{\mathbf{q}}) (\mathcal{H}^{-1} \Phi'_{\mathbf{k}-\mathbf{q}} + \Phi_{\mathbf{k}-\mathbf{q}}) \right]. \quad (24)$$

During the radiation-dominated era, the scalar perturbation satisfies the following equation of motion in Fourier space to be expressed as

$$\Phi_k'' + 4\mathcal{H}\Phi_k' - \frac{k^3}{3}\Phi_k = 0, \quad (25)$$

where  $\Phi_{\mathbf{k}}$  is the Fourier component of the gravitational potential, and it can be related to its primordial value  $\phi_k$  by the transfer function

$$\Phi_{\mathbf{k}} = \Phi(k\eta)\phi_{\mathbf{k}}. \quad (26)$$

The transfer function for the radiation-dominated period is given by

$$\Phi(k\eta) = \frac{9}{(k\eta)^2} \left( \frac{\sin(k\eta/\sqrt{3})}{k\eta/\sqrt{3}} - \cos(k\eta/\sqrt{3}) \right), \quad (27)$$

and its two-point correlation function is determined by the power spectrum of the curvature perturbation

$$\langle \phi_{\mathbf{k}} \phi_{\mathbf{k}'} \rangle = \delta(\mathbf{k} + \mathbf{k}') \frac{2\pi^2}{k^3} \left( \frac{3 + 3w}{5 + 3w} \right)^2 P_{\zeta}(k). \quad (28)$$

The power spectrum of induced gravitational waves can be written as

$$\langle h_{\mathbf{k}}^{\lambda}(\eta) h_{\mathbf{k}'}^{\lambda'}(\eta) \rangle = \delta_{\lambda\lambda'} \delta^{(3)}(\mathbf{k} + \mathbf{k}') \frac{2\pi^2}{k^3} P_h(k, \eta), \quad (29)$$

where  $\lambda, \lambda' = +, \times$  represents the polarization index, which we omit in the following. We solve the tensor Eq. (23) by employing the Green's function method, we obtain  $h_{\mathbf{k}}(\eta)$  is expressed as

$$h_{\mathbf{k}}(\eta) = \frac{4}{a(\eta)} \int^{\eta} d\bar{\eta} G_k(\eta, \bar{\eta}) a(\bar{\eta}) S_{\mathbf{k}}(\bar{\eta}), \quad (30)$$

during the radiation-dominated period, the Green's function of GW is

$$G_k(\eta, \bar{\eta}) = \frac{\sin[k(\eta - \bar{\eta})]}{k}. \quad (31)$$

The fraction of the GW energy density is [90, 93]

$$\Omega_{\text{GW}}(k, \eta) = \frac{1}{24} \left( \frac{k}{a(\eta)H(\eta)} \right)^2 \overline{P_h(k, \eta)}. \quad (32)$$

Substituting the solution Eq. (30) into Eq. (29), we calculated the power spectrum for the SIGWs  $P_h$  is brought into Eq. (32) to obtain the fraction of energy density [90, 94]

$$\Omega_{\text{GW}}(k) = \frac{1}{6} \left( \frac{k}{aH} \right)^2 \int_0^{\infty} dv \int_{|1-v|}^{1+v} du \left\{ \left[ \frac{4v^2 - (1-u^2+v^2)^2}{4uv} \right]^2 \times I_R^2(u, v, x \rightarrow \infty) \mathcal{P}_{\zeta}(kv) \mathcal{P}_{\zeta}(ku) \right\}, \quad (33)$$

where  $u = |\mathbf{k} - \tilde{\mathbf{k}}|$ ,  $v = \tilde{k}/k$ ,  $x = k\eta$ , and  $I_R$  is kernel function. The current frequency  $f$  and wave number  $k$  of the induced gravitational wave satisfy the following equation [95]

$$f = 1.546 \times 10^{-15} \frac{k}{1\text{Mpc}^{-1}} \text{Hz}. \quad (34)$$

The fractional energy density of SIGWs today

$$\Omega_{\text{GW},0}(k) = \frac{\Omega_{\text{r},0}(k)}{\Omega_{\text{r}}(k)} \Omega_{\text{GW}}(k) \quad (35)$$

where  $\Omega_{\text{r},0}(k) = 9.17 \times 10^{-5}$  is the current fractional energy density of radiation, and we choose  $\Omega_{\text{r}}(k) = 1$  during the radiation domination [37, 96]. By substituting the numerical results of the power spectrum into Eq. (35), we obtain the energy density  $\Omega_{\text{GW},0}$  of the SIGWs for the corresponding models, and the peak frequencies  $f_c$  of these SIGWs are shown in Table I.

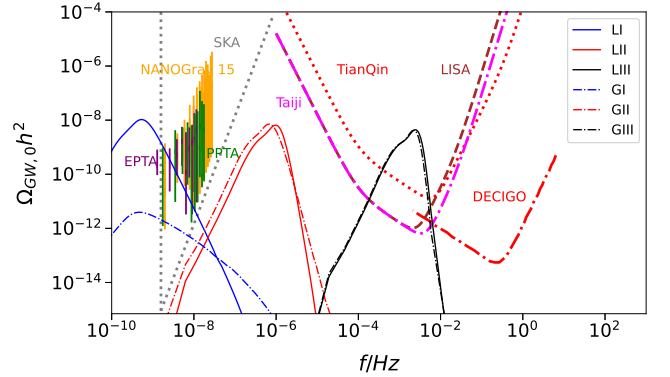


FIG. 7: The energy density spectrum of SIGWs. The curves show the sensitivity of current and future GW observatories. The purple dashed curve, the green dot-dashed curve and the orange dotted curve denote the EPTA DR2full limit [62], PPTA DR3 limit [63] and the SKA limit [97], respectively. The other limits from the TianQin [66], Taiji [65], the DECIGO [67], the LISA [64] and the aLIGO [1, 2], respectively. The blue region is the observational result from the North American Nanohertz Observatory for Gravitational Wave (NANOGrav) 15-year data [61].

In this part, we show the predictions of the energy density spectrum of GWs for the above-mentioned parameters in Fig. 7 and compare them with the constraints and future sensitivity curves for the GW observatories.

As for the parameter set LI, the consequent SIGWs can explain the NANOGrav 15yrs signal and can be tested by EPTA/PPTA/SKA. Here, because the power spectrum for set GI is small, the energy density of SIGWs is also small as shown in Fig. 7, which can be tested by PPTA/SKA. However, nHz SIGWs could be located within the range of the NANOGrav 15yrs data set, and also have a narrower frequency range than LI. As for the parameter sets LIII and GIII, the SIGWs can be tested by LISA/Taiji/TianQin/ DECIGO.

## V. CONCLUSION AND DISCUSSION

In this paper, we focus on the generation of PBHs and SIGWs within an inflation potential bump. We propose a simple Lorentz function form of bump as a local correction of the basis inflation potential, which can enhance the power spectrum of the primordial curvature perturbation to  $\mathcal{O}(10^{-2})$  and satisfy the prerequisites for generating PBHs. At the same time, our numerical results for the scalar spectral index  $n_s$  and tensor-to-scalar ratio  $r$  predicted by this model align with the Planck 2018 results.

Subsequently, we calculate the abundance of PBHs and the energy density of SIGWs produced by the Lorentz and Gaussian bumps. The PBHs with mass  $10^{-12}M_\odot$  can make up almost all dark matter, and PBHs with mass  $10^{-5}M_\odot$  can explain OGLE ultrashort-timescale microlensing events and can be explained to Planet 9. The process of PBH formation could be concomitant with the generation of SIGWs. We obtain these SIGWs that can be tested by GW observatories, i.e., PTA, SKA, Tianqin, Taiji, LISA, and DECIGO. The nHz SIGWs for our models can be located within the range of the NANOGrav 15yrs data set.

This paper compares the Gaussian bump form with the Lorentz bump case. Moreover, we also give numerical results for the Hyperbolic bump form in the Appendix A. From the results, We find that the Gaussian and Hyperbolic cases do not produce sufficient abundance for PBH with stellar mass, while the Lorentz function bump cases do. The frequency range of nHz SIGWs that can be tested is wider from Lorentz's case. Therefore, our paper provides a simple example, which implies the Lorentz function bump presents more advantages for a basic potential function with large  $N$ .

Many intriguing aspects could be extended in the future. Recently, many studies have indicated that enhancements in the power spectrum of curvature perturbations at small scales can lead to significant loop corrections at the CMB scale, which thereby disrupt the research information mechanism of PBHs [98, 99]. Subsequently, it has been recognized that one-loop corrections can be suppressed in cases where the transition to slow rolling expansion is smooth [100–103]. Naturally, a similar one-loop correction can be contemplated within the framework of our model and left for future study.

Moreover, there are two most common methods to

calculate the mass function  $\beta$ . We have used the Press-Schechter (PS) theory to calculate in our present study [85]. The other peak theory method was first proposed by Ref. [104]. In reference [105], Green estimated the abundance of PBHs by simplifying the peak theory. Under certain conditions, their conclusions are consistent with the PS theory [85]. However, it's important to note that the PBHs abundance predicted by the PS theory is  $2 \sim 3$  orders of magnitude lower than the peak theory employed by the researchers [69]. This significant difference underscores the importance of further exploring and comparing the two methods for calculating PBHs abundance with our model in the future.

Furthermore, one feature of the USR violates Maldacena's non-Gaussian consistency relation  $f_{\text{NL}} = 5/12(1 - n_s)$ , which connects the squeezed limit of the bispectrum to the power spectrum [74]. It has also been shown that the significant non-Gaussianity generated by the USR phase can be partially or eliminated by this transition phase, although Maldacena's consistency relation remains violated [106]. However, Ref. [107–109] present varied findings concerning the non-Gaussian properties linked with non-attractor models. Furthermore, the quantum stochastic effects during the USR phase could influence the amplification of curvature perturbations [110–112]. Due to the aforementioned uncertainties, we have neglected non-Gaussianity and quantum stochastic effects in our analysis for simplicity. Future studies could include these effects to obtain more precise results for PBHs formation with our bump potential [113–117].

## Acknowledgements

We appreciate very much the insightful comments and helpful suggestions by the anonymous referee. We would like to thank Profs. Bum-Hoon Lee, Shi Pi, and Dr. Zhu Yi for their useful discussions. We are also grateful to our group members for their assistance. This work is supported by the National Natural Science Foundation of China (NSFC) under Grant No. 12175105, No. 11575083, No. 11565017, No. 12147175, Ya-Peng Hu is supported by the Top-notch Academic Programs Project of Jiangsu Higher Education Institutions (TAPP).

## Appendix A: Hyperbolic function bump

The Starobinsky inflation model with Hyperbolic function bump is written as

$$V_{\text{H}}(\phi) = \frac{3}{4}m^2 \left(1 - e^{-\sqrt{\frac{2}{3}}\phi}\right)^2 \left(1 + \frac{b}{\cosh^2\left(\frac{\phi-\phi_0}{c}\right)}\right). \quad (\text{A1})$$

We numerically calculate the result of the power spectrum with the Hyperbolic bump in  $\phi_0 = 5.1$ , whose



maximum power spectrum at this position is similar to that of the Gaussian case, as shown in Fig. 8 HI.

Moreover, the power spectrum for set HI cannot reach  $\mathcal{O}(10^{-2})$ , their PBHs abundance is approximately 0, and can not produce a sufficient abundance of PBHs with stellar mass as shown in Fig. 9. For SIGWs in Fig. 10, we can see that the energy density of their corresponding SIGWs is relatively low. Several other sets are similar to Lorentz functions LII and LIII. From the above calculation results, the Lorentz bump shows more advantages in PBHs and SIGWs formation than the Gaussian and Hyperbolic bump forms. The relevant data are recorded in Table II.

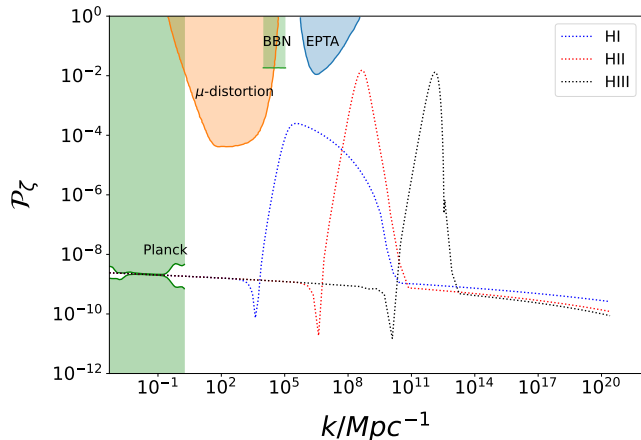


FIG. 8: The scalar power spectrum for Hyperbolic bump.

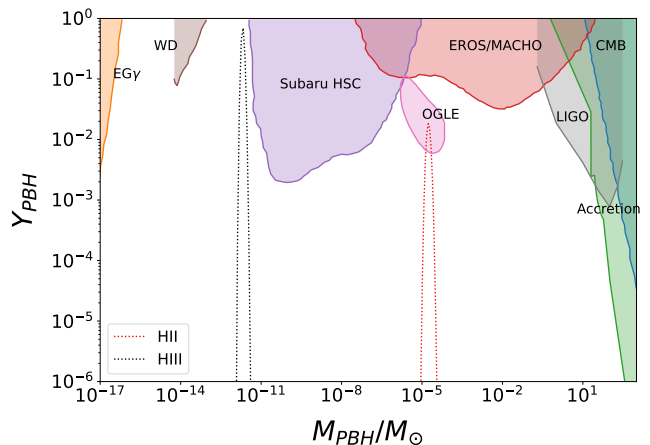


FIG. 9: The abundances of PBHs produced for Hyperbolic bump.

- [1] B. P. Abbott et al. (LIGO Scientific, Virgo), Observation of Gravitational Waves from a Binary Black Hole Merger, *Phys. Rev. Lett.* **116**, 061102 (2016), [arXiv:1602.03837 \[gr-qc\]](#).
- [2] B. P. Abbott et al. (LIGO Scientific, Virgo), GWTC-1: A Gravitational-Wave Transient Catalog of Compact Binary Mergers Observed by LIGO and Virgo during the First and Second Observing Runs, *Phys. Rev. X* **9**, 031040 (2019), [arXiv:1811.12907 \[astro-ph.HE\]](#).
- [3] S. Bird, I. Cholis, J. B. Muñoz, Y. Ali-Haïmoud, M. Kamionkowski, E. D. Kovetz, A. Raccanelli, and A. G. Riess, Did LIGO detect dark matter?, *Phys. Rev. Lett.* **116**, 201301 (2016), [arXiv:1603.00464 \[astro-ph.CO\]](#).
- [4] M. Sasaki, T. Suyama, T. Tanaka, and S. Yokoyama, Primordial Black Hole Scenario for the Gravitational-Wave Event GW150914, *Phys. Rev. Lett.* **117**, 061101 (2016), [Erratum: *Phys.Rev.Lett.* 121, 059901 (2018)], [arXiv:1603.08338 \[astro-ph.CO\]](#).
- [5] G. F. Chapline, Cosmological effects of primordial black holes, *Nature* **253**, 251 (1975).
- [6] V. C. Rubin, N. Thonnard, and W. K. Ford, Jr., Rotational properties of 21 SC galaxies with a large range of luminosities and radii, from NGC 4605 /R = 4kpc/ to UGC 2885 /R = 122 kpc/, *Astrophys. J.* **238**, 471 (1980).

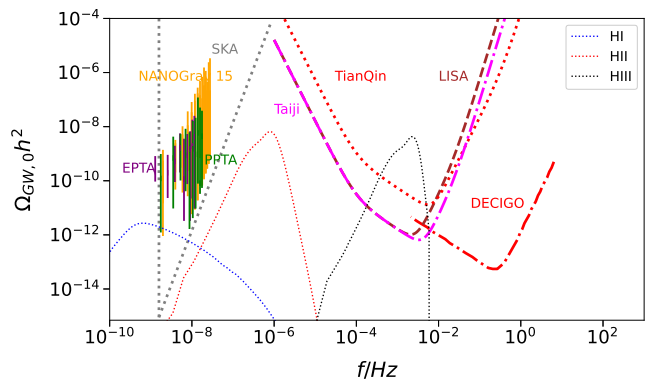


FIG. 10: The energy density spectrum of SIGWs for Hyperbolic bump.

- [7] M. Persic, P. Salucci, and F. Stel, The Universal rotation curve of spiral galaxies: 1. The Dark matter connection, *Mon. Not. Roy. Astron. Soc.* **281**, 27 (1996), [arXiv:astro-ph/9506004](#).
- [8] G. Bertone and D. Hooper, History of dark matter, *Rev. Mod. Phys.* **90**, 045002 (2018), [arXiv:1605.04909 \[astro-ph.CO\]](#).

TABLE II: Model parameters and the numerical results for Hyperbolic bump

<i>set</i>	$b(10^{-4})$	$c$	$\phi_0$	$N$	$n_s$	$r$	$k_{\text{peak}}/\text{Mpc}^{-1}$	$P_{\zeta(\text{peak})}$	$\frac{M_{\text{peak}}}{M_{\odot}}$	$Y_{\text{PBH}}^{\text{peak}}$	$f_c/\text{Hz}$
<i>HI</i>	4.3175	0.013	5.1	70	0.9678	0.003	$3.51 \times 10^5$	0.00024	29.8	0	$5.9 \times 10^{-10}$
<i>HII</i>	3.87382	0.009	4.89	63	0.9678	0.003	$4.63 \times 10^8$	0.015	$1.71 \times 10^{-5}$	0.18	$7 \times 10^{-7}$
<i>HIII</i>	3.93309	0.0054	4.63	61	0.9678	0.003	$1.31 \times 10^{12}$	0.013	$2.15 \times 10^{-12}$	0.69	$2.2 \times 10^{-3}$

- [9] P. H. Frampton, M. Kawasaki, F. Takahashi, and T. T. Yanagida, Primordial Black Holes as All Dark Matter, *JCAP* **04**, 023 (2010), [arXiv:1001.2308 \[hep-ph\]](#) .
- [10] S. Clesse and J. García-Bellido, Massive Primordial Black Holes from Hybrid Inflation as Dark Matter and the seeds of Galaxies, *Phys. Rev. D* **92**, 023524 (2015), [arXiv:1501.07565 \[astro-ph.CO\]](#) .
- [11] K. Inomata, M. Kawasaki, K. Mukaida, Y. Tada, and T. T. Yanagida, Inflationary Primordial Black Holes as All Dark Matter, *Phys. Rev. D* **96**, 043504 (2017), [arXiv:1701.02544 \[astro-ph.CO\]](#) .
- [12] J. García-Bellido, Massive Primordial Black Holes as Dark Matter and their detection with Gravitational Waves, *J. Phys. Conf. Ser.* **840**, 012032 (2017), [arXiv:1702.08275 \[astro-ph.CO\]](#) .
- [13] E. D. Kovetz, Probing Primordial-Black-Hole Dark Matter with Gravitational Waves, *Phys. Rev. Lett.* **119**, 131301 (2017), [arXiv:1705.09182 \[astro-ph.CO\]](#) .
- [14] B. Carr, F. Kuhnel, and M. Sandstad, Primordial Black Holes as Dark Matter, *Phys. Rev. D* **94**, 083504 (2016), [arXiv:1607.06077 \[astro-ph.CO\]](#) .
- [15] B. Carr, K. Kohri, Y. Sendouda, and J. Yokoyama, Constraints on primordial black holes, *Rept. Prog. Phys.* **84**, 116902 (2021), [arXiv:2002.12778 \[astro-ph.CO\]](#) .
- [16] B. Carr and F. Kuhnel, Primordial Black Holes as Dark Matter: Recent Developments, *Ann. Rev. Nucl. Part. Sci.* **70**, 355 (2020), [arXiv:2006.02838 \[astro-ph.CO\]](#) .
- [17] M. Y. Khlopov, Primordial Black Holes, *Res. Astron. Astrophys.* **10**, 495 (2010), [arXiv:0801.0116 \[astro-ph\]](#) .
- [18] Y. Ali-Haïmoud and M. Kamionkowski, Cosmic microwave background limits on accreting primordial black holes, *Phys. Rev. D* **95**, 043534 (2017), [arXiv:1612.05644 \[astro-ph.CO\]](#) .
- [19] V. Poulin, P. D. Serpico, F. Calore, S. Clesse, and K. Kohri, CMB bounds on disk-accreting massive primordial black holes, *Phys. Rev. D* **96**, 083524 (2017), [arXiv:1707.04206 \[astro-ph.CO\]](#) .
- [20] B. J. Carr, K. Kohri, Y. Sendouda, and J. Yokoyama, New cosmological constraints on primordial black holes, *Phys. Rev. D* **81**, 104019 (2010), [arXiv:0912.5297 \[astro-ph.CO\]](#) .
- [21] P. W. Graham, S. Rajendran, and J. Varela, Dark Matter Triggers of Supernovae, *Phys. Rev. D* **92**, 063007 (2015), [arXiv:1505.04444 \[hep-ph\]](#) .
- [22] H. Niikura et al., Microlensing constraints on primordial black holes with Subaru/HSC Andromeda observations, *Nature Astron.* **3**, 524 (2019), [arXiv:1701.02151 \[astro-ph.CO\]](#) .
- [23] K. Griest, A. M. Cieplak, and M. J. Lehner, New Limits on Primordial Black Hole Dark Matter from an Analysis of Kepler Source Microlensing Data, *Phys. Rev. Lett.* **111**, 181302 (2013).
- [24] P. Tisserand et al. (EROS-2), Limits on the Macho Content of the Galactic Halo from the EROS-2 Survey of the Magellanic Clouds, *Astron. Astrophys.* **469**, 387 (2007), [arXiv:astro-ph/0607207](#) .
- [25] V. Vaskonen and H. Veermäe, Lower bound on the primordial black hole merger rate, *Phys. Rev. D* **101**, 043015 (2020).
- [26] A. M. Green and B. J. Kavanagh, Primordial Black Holes as a dark matter candidate, *J. Phys. G* **48**, 043001 (2021), [arXiv:2007.10722 \[astro-ph.CO\]](#) .
- [27] H. Niikura, M. Takada, S. Yokoyama, T. Sumi, and S. Masaki, Constraints on Earth-mass primordial black holes from OGLE 5-year microlensing events, *Phys. Rev. D* **99**, 083503 (2019).
- [28] P. Mróz, A. Udalski, J. Skowron, R. Poleski, S. Kozłowski, M. K. Szymański, I. Soszyński, Ł. Wyrzykowski, P. Pietrukowicz, K. Ulaczyk, D. Skowron, and M. Pawlak, No large population of unbound or wide-orbit Jupiter-mass planets, *Nature (London)* **548**, 183 (2017), [arXiv:1707.07634 \[astro-ph.EP\]](#) .
- [29] S. Hawking, Gravitationally collapsed objects of very low mass, *Mon. Not. Roy. Astron. Soc.* **152**, 75 (1971).
- [30] P. Ivanov, P. Naselsky, and I. Novikov, Inflation and primordial black holes as dark matter, *Phys. Rev. D* **50**, 7173 (1994).
- [31] J. Garcia-Bellido and E. Ruiz Morales, Primordial black holes from single field models of inflation, *Phys. Dark Univ.* **18**, 47 (2017), [arXiv:1702.03901 \[astro-ph.CO\]](#) .
- [32] H. Di and Y. Gong, Primordial black holes and second order gravitational waves from ultra-slow-roll inflation, *JCAP* **07**, 007 (2018), [arXiv:1707.09578 \[astro-ph.CO\]](#) .
- [33] M. Sasaki, T. Suyama, T. Tanaka, and S. Yokoyama, Primordial black holes—perspectives in gravitational wave astronomy, *Class. Quant. Grav.* **35**, 063001 (2018), [arXiv:1801.05235 \[astro-ph.CO\]](#) .
- [34] S. Pi and J. Wang, Primordial black hole formation in Starobinsky’s linear potential model, *JCAP* **06**, 018 (2023), [arXiv:2209.14183 \[astro-ph.CO\]](#) .
- [35] W.-T. Xu, J. Liu, T.-J. Gao, and Z.-K. Guo, Gravitational waves from double-inflection-point inflation, *Phys. Rev. D* **101**, 023505 (2020), [arXiv:1907.05213 \[astro-ph.CO\]](#) .
- [36] L. Anguelova, On Primordial Black Holes from Rapid Turns in Two-field Models, *JCAP* **06**, 004 (2021), [arXiv:2012.03705 \[hep-th\]](#) .
- [37] Z. Yi, Q. Gao, Y. Gong, and Z.-h. Zhu, Primordial black holes and scalar-induced secondary gravitational waves from inflationary models with a noncanonical kinetic term, *Phys. Rev. D* **103**, 063534 (2021), [arXiv:2011.10606 \[astro-ph.CO\]](#) .
- [38] C. Chen, A. Ghoshal, Z. Lalak, Y. Luo, and A. Naskar, Growth of curvature perturbations for PBH formation & detectable GWs in non-minimal curvaton scenario

- revisited, JCAP **08**, 041 (2023), [arXiv:2305.12325 \[astro-ph.CO\]](#) .
- [39] S. Pi and M. Sasaki, Primordial black hole formation in nonminimal curvaton scenarios, Phys. Rev. D **108**, L101301 (2023), [arXiv:2112.12680 \[astro-ph.CO\]](#) .
- [40] T. Papanikolaou, A. Lympferis, S. Lola, and E. N. Saridakis, Primordial black holes and gravitational waves from non-canonical inflation, JCAP **03**, 003 (2023), [arXiv:2211.14900 \[astro-ph.CO\]](#) .
- [41] L. Wu, Y. Gong, and T. Li, Primordial black holes and secondary gravitational waves from string inspired general no-scale supergravity, Phys. Rev. D **104**, 123544 (2021), [arXiv:2105.07694 \[gr-qc\]](#) .
- [42] S. Kawai and J. Kim, Primordial black holes from Gauss-Bonnet-corrected single field inflation, Phys. Rev. D **104**, 083545 (2021), [arXiv:2108.01340 \[astro-ph.CO\]](#) .
- [43] S. Kawai and J. Kim, Primordial black holes and gravitational waves from nonminimally coupled supergravity inflation, Phys. Rev. D **107**, 043523 (2023), [arXiv:2209.15343 \[astro-ph.CO\]](#) .
- [44] J. Garriga and A. Vilenkin, Black holes from nucleating strings, Phys. Rev. D **47**, 3265 (1993), [arXiv:hep-ph/9208212](#) .
- [45] A. Polnarev and R. Zembowicz, Formation of Primordial Black Holes by Cosmic Strings, Phys. Rev. D **43**, 1106 (1991).
- [46] H. Deng, J. Garriga, and A. Vilenkin, Primordial black hole and wormhole formation by domain walls, JCAP **04**, 050 (2017), [arXiv:1612.03753 \[gr-qc\]](#) .
- [47] Y. N. Eroshenko, Spin of primordial black holes in the model with collapsing domain walls, JCAP **12**, 041 (2021), [arXiv:2111.03403 \[astro-ph.CO\]](#) .
- [48] M. Lewicki, P. Toczek, and V. Vaskonen, Primordial black holes from strong first-order phase transitions, JHEP **09**, 092 (2023), [arXiv:2305.04924 \[astro-ph.CO\]](#) .
- [49] J. Liu, L. Bian, R.-G. Cai, Z.-K. Guo, and S.-J. Wang, Primordial black hole production during first-order phase transitions, Phys. Rev. D **105**, L021303 (2022), [arXiv:2106.05637 \[astro-ph.CO\]](#) .
- [50] R. Saito and J. Yokoyama, Gravitational wave background as a probe of the primordial black hole abundance, Phys. Rev. Lett. **102**, 161101 (2009), [Erratum: Phys.Rev.Lett. 107, 069901 (2011)], [arXiv:0812.4339 \[astro-ph\]](#) .
- [51] R. Saito and J. Yokoyama, Gravitational-Wave Constraints on the Abundance of Primordial Black Holes, Prog. Theor. Phys. **123**, 867 (2010), [Erratum: Prog.Theor.Phys. 126, 351–352 (2011)], [arXiv:0912.5317 \[astro-ph.CO\]](#) .
- [52] N. Orlofsky, A. Pierce, and J. D. Wells, Inflationary theory and pulsar timing investigations of primordial black holes and gravitational waves, Phys. Rev. D **95**, 063518 (2017), [arXiv:1612.05279 \[astro-ph.CO\]](#) .
- [53] S. Wang, Y.-F. Wang, Q.-G. Huang, and T. G. F. Li, Constraints on the Primordial Black Hole Abundance from the First Advanced LIGO Observation Run Using the Stochastic Gravitational-Wave Background, Phys. Rev. Lett. **120**, 191102 (2018), [arXiv:1610.08725 \[astro-ph.CO\]](#) .
- [54] R.-g. Cai, S. Pi, and M. Sasaki, Gravitational Waves Induced by non-Gaussian Scalar Perturbations, Phys. Rev. Lett. **122**, 201101 (2019), [arXiv:1810.11000 \[astro-ph.CO\]](#) .
- [55] Z. Yi, Primordial black holes and scalar-induced gravitational waves from the generalized Brans-Dicke theory, JCAP **03**, 048 (2023), [arXiv:2206.01039 \[gr-qc\]](#) .
- [56] G. Domènech, Scalar Induced Gravitational Waves Review, Universe **7**, 398 (2021), [arXiv:2109.01398 \[gr-qc\]](#) .
- [57] K. Inomata, K. Kohri, and T. Terada, Detected stochastic gravitational waves and subsolar-mass primordial black holes, Phys. Rev. D **109**, 063506 (2024), [arXiv:2306.17834 \[astro-ph.CO\]](#) .
- [58] K. Kohri and T. Terada, Solar-Mass Primordial Black Holes Explain NANOGrav Hint of Gravitational Waves, Phys. Lett. B **813**, 136040 (2021), [arXiv:2009.11853 \[astro-ph.CO\]](#) .
- [59] S. Basilakos, D. V. Nanopoulos, T. Papanikolaou, E. N. Saridakis, and C. Tzerefos, Induced gravitational waves from flipped SU(5) superstring theory at nHz, Phys. Lett. B **849**, 138446 (2024), [arXiv:2309.15820 \[astro-ph.CO\]](#) .
- [60] S. Basilakos, D. V. Nanopoulos, T. Papanikolaou, E. N. Saridakis, and C. Tzerefos, Gravitational wave signatures of no-scale supergravity in NANOGrav and beyond, Phys. Lett. B **850**, 138507 (2024), [arXiv:2307.08601 \[hep-th\]](#) .
- [61] G. Agazie et al. (NANOGrav), The NANOGrav 15 yr Data Set: Evidence for a Gravitational-wave Background, Astrophys. J. Lett. **951**, L8 (2023), [arXiv:2306.16213 \[astro-ph.HE\]](#) .
- [62] J. Antoniadis et al. (EPTA, InPTA:), The second data release from the European Pulsar Timing Array - III. Search for gravitational wave signals, Astron. Astrophys. **678**, A50 (2023), [arXiv:2306.16214 \[astro-ph.HE\]](#) .
- [63] D. J. Reardon et al., Search for an Isotropic Gravitational-wave Background with the Parkes Pulsar Timing Array, Astrophys. J. Lett. **951**, L6 (2023), [arXiv:2306.16215 \[astro-ph.HE\]](#) .
- [64] P. Amaro-Seoane et al. (LISA), Laser Interferometer Space Antenna, (2017), [arXiv:1702.00786 \[astro-ph.IM\]](#) .
- [65] W.-R. Hu and Y.-L. Wu, The Taiji Program in Space for gravitational wave physics and the nature of gravity, Natl. Sci. Rev. **4**, 685 (2017).
- [66] J. Luo et al. (TianQin), TianQin: a space-borne gravitational wave detector, Class. Quant. Grav. **33**, 035010 (2016), [arXiv:1512.02076 \[astro-ph.IM\]](#) .
- [67] S. Kawamura et al., The Japanese space gravitational wave antenna DECIGO, Class. Quant. Grav. **23**, S125 (2006).
- [68] C. Fu and C. Chen, Sudden braking and turning with a two-field potential bump: primordial black hole formation, JCAP **05**, 005 (2023), [arXiv:2211.11387 \[astro-ph.CO\]](#) .
- [69] Q. Wang, Y.-C. Liu, B.-Y. Su, and N. Li, Primordial black holes from the perturbations in the inflaton potential in peak theory, Phys. Rev. D **104**, 083546 (2021), [arXiv:2111.10028 \[astro-ph.CO\]](#) .
- [70] J.-X. Zhao, X.-H. Liu, and N. Li, Primordial black holes and scalar-induced gravitational waves from the perturbations on the inflaton potential in peak theory, Phys. Rev. D **107**, 043515 (2023), [arXiv:2302.06886 \[astro-ph.CO\]](#) .
- [71] S. S. Mishra and V. Sahni, Primordial Black Holes from a tiny bump/dip in the Inflaton potential, JCAP **04**, 007 (2020), [arXiv:1911.00057 \[gr-qc\]](#) .
- [72] A. A. Starobinsky, A New Type of Isotropic Cosmological Models Without Singularity, Phys. Lett. B **91**, 99 (1980).

- [73] S. S. Mishra, V. Sahni, and A. V. Toporensky, Initial conditions for Inflation in an FRW Universe, *Phys. Rev. D* **98**, 083538 (2018), [arXiv:1801.04948 \[gr-qc\]](#) .
- [74] J. M. Maldacena, Non-Gaussian features of primordial fluctuations in single field inflationary models, *JHEP* **05**, 013 (2003), [arXiv:astro-ph/0210603](#) .
- [75] V. F. Mukhanov, Gravitational Instability of the Universe Filled with a Scalar Field, *JETP Lett.* **41**, 493 (1985).
- [76] M. Sasaki, Large Scale Quantum Fluctuations in the Inflationary Universe, *Prog. Theor. Phys.* **76**, 1036 (1986).
- [77] Y. Akrami et al. (Planck), Planck 2018 results. X. Constraints on inflation, *Astron. Astrophys.* **641**, A10 (2020), [arXiv:1807.06211 \[astro-ph.CO\]](#) .
- [78] K. Inomata and T. Nakama, Gravitational waves induced by scalar perturbations as probes of the small-scale primordial spectrum, *Phys. Rev. D* **99**, 043511 (2019), [arXiv:1812.00674 \[astro-ph.CO\]](#) .
- [79] K. Inomata, M. Kawasaki, and Y. Tada, Revisiting constraints on small scale perturbations from big-bang nucleosynthesis, *Phys. Rev. D* **94**, 043527 (2016), [arXiv:1605.04646 \[astro-ph.CO\]](#) .
- [80] D. J. Fixsen, E. S. Cheng, J. M. Gales, J. C. Mather, R. A. Shafer, and E. L. Wright, The Cosmic Microwave Background spectrum from the full COBE FIRAS data set, *Astrophys. J.* **473**, 576 (1996), [arXiv:astro-ph/9605054](#) .
- [81] J. Chluba, A. L. Erickcek, and I. Ben-Dayan, Probing the Inflaton: Small-scale Power Spectrum Constraints from Measurements of the Cosmic Microwave Background Energy Spectrum, *Astrophys. J.* **758**, 76 (2012), [arXiv:1203.2681 \[astro-ph.CO\]](#) .
- [82] D. Jeong, J. Pradler, J. Chluba, and M. Kamionkowski, Silk Damping at a Redshift of a Billion: New Limit on Small-Scale Adiabatic Perturbations, *Phys. Rev. Lett.* **113**, 061301 (2014), [arXiv:1403.3697 \[astro-ph.CO\]](#) .
- [83] P. A. R. Ade et al. (BICEP2, Keck Array), BICEP2 / Keck Array x: Constraints on Primordial Gravitational Waves using Planck, WMAP, and New BICEP2/Keck Observations through the 2015 Season, *Phys. Rev. Lett.* **121**, 221301 (2018), [arXiv:1810.05216 \[astro-ph.CO\]](#) .
- [84] P. A. R. Ade et al. (BICEP, Keck), Improved Constraints on Primordial Gravitational Waves using Planck, WMAP, and BICEP/Keck Observations through the 2018 Observing Season, *Phys. Rev. Lett.* **127**, 151301 (2021), [arXiv:2110.00483 \[astro-ph.CO\]](#) .
- [85] W. H. Press and P. Schechter, Formation of galaxies and clusters of galaxies by self-similar gravitational condensation, *Astrophys. J.* **187**, 425 (1974).
- [86] T. Harada, C.-M. Yoo, and K. Kohri, Threshold of primordial black hole formation, *Phys. Rev. D* **88**, 084051 (2013), [Erratum: *Phys.Rev.D* 89, 029903 (2014)], [arXiv:1309.4201 \[astro-ph.CO\]](#) .
- [87] B. J. Carr, The Primordial black hole mass spectrum, *Astrophys. J.* **201**, 1 (1975).
- [88] N. Aghanim et al. (Planck), Planck 2018 results. VI. Cosmological parameters, *Astron. Astrophys.* **641**, A6 (2020), [Erratum: *Astron.Astrophys.* 652, C4 (2021)], [arXiv:1807.06209 \[astro-ph.CO\]](#) .
- [89] J. Scholtz and J. Unwin, What if Planet 9 is a Primordial Black Hole?, *Phys. Rev. Lett.* **125**, 051103 (2020), [arXiv:1909.11090 \[hep-ph\]](#) .
- [90] K. Kohri and T. Terada, Semianalytic calculation of gravitational wave spectrum nonlinearly induced from primordial curvature perturbations, *Phys. Rev. D* **97**, 123532 (2018), [arXiv:1804.08577 \[gr-qc\]](#) .
- [91] K. N. Ananda, C. Clarkson, and D. Wands, The Cosmological gravitational wave background from primordial density perturbations, *Phys. Rev. D* **75**, 123518 (2007), [arXiv:gr-qc/0612013](#) .
- [92] D. Baumann, P. J. Steinhardt, K. Takahashi, and K. Ichiki, Gravitational Wave Spectrum Induced by Primordial Scalar Perturbations, *Phys. Rev. D* **76**, 084019 (2007), [arXiv:hep-th/0703290](#) .
- [93] A. Ali, Y.-P. Hu, M. Sabir, and T. Sui, On the gauge dependence of scalar induced secondary gravitational waves during radiation and matter domination eras, *Sci. China Phys. Mech. Astron.* **66**, 290411 (2023), [arXiv:2308.04713 \[gr-qc\]](#) .
- [94] Y. Lu, A. Ali, Y. Gong, J. Lin, and F. Zhang, Gauge transformation of scalar induced gravitational waves, *Phys. Rev. D* **102**, 083503 (2020), [arXiv:2006.03450 \[gr-qc\]](#) .
- [95] C. Fu, P. Wu, and H. Yu, Scalar induced gravitational waves in inflation with gravitationally enhanced friction, *Phys. Rev. D* **101**, 023529 (2020), [arXiv:1912.05927 \[astro-ph.CO\]](#) .
- [96] F. Zhang, Primordial black holes and scalar induced gravitational waves from the E model with a Gauss-Bonnet term, *Phys. Rev. D* **105**, 063539 (2022), [arXiv:2112.10516 \[gr-qc\]](#) .
- [97] C. J. Moore, R. H. Cole, and C. P. L. Berry, Gravitational-wave sensitivity curves, *Class. Quant. Grav.* **32**, 015014 (2015), [arXiv:1408.0740 \[gr-qc\]](#) .
- [98] J. Kristiano and J. Yokoyama, Constraining Primordial Black Hole Formation from Single-Field Inflation, *Phys. Rev. Lett.* **132**, 221003 (2024), [arXiv:2211.03395 \[hep-th\]](#) .
- [99] J. Kristiano and J. Yokoyama, Note on the bispectrum and one-loop corrections in single-field inflation with primordial black hole formation, *Phys. Rev. D* **109**, 103541 (2024), [arXiv:2303.00341 \[hep-th\]](#) .
- [100] A. Riotto, The Primordial Black Hole Formation from Single-Field Inflation is Still Not Ruled Out, (2023), [arXiv:2303.01727 \[astro-ph.CO\]](#) .
- [101] H. Firouzjahi, One-loop corrections in power spectrum in single field inflation, *JCAP* **10**, 006 (2023), [arXiv:2303.12025 \[astro-ph.CO\]](#) .
- [102] H. Firouzjahi and A. Riotto, Primordial Black Holes and loops in single-field inflation, *JCAP* **02**, 021 (2024), [arXiv:2304.07801 \[astro-ph.CO\]](#) .
- [103] H. Firouzjahi, Revisiting loop corrections in single field ultraslow-roll inflation, *Phys. Rev. D* **109**, 043514 (2024), [arXiv:2311.04080 \[astro-ph.CO\]](#) .
- [104] J. M. Bardeen, J. R. Bond, N. Kaiser, and A. S. Szalay, The Statistics of Peaks of Gaussian Random Fields, *Astrophys. J.* **304**, 15 (1986).
- [105] A. M. Green, A. R. Liddle, K. A. Malik, and M. Sasaki, A New calculation of the mass fraction of primordial black holes, *Phys. Rev. D* **70**, 041502 (2004), [arXiv:astro-ph/0403181](#) .
- [106] Y.-F. Cai, X. Chen, M. H. Namjoo, M. Sasaki, D.-G. Wang, and Z. Wang, Revisiting non-Gaussianity from non-attractor inflation models, *JCAP* **05**, 012 (2018), [arXiv:1712.09998 \[astro-ph.CO\]](#) .
- [107] S. Passaglia, W. Hu, and H. Motohashi, Primordial black holes and local non-Gaussianity in canonical inflation, *Phys. Rev. D* **99**, 043536 (2019), [arXiv:1812.08243 \[astro-ph.CO\]](#) .

- [ph.CO](#)].
- [108] R. Bravo, S. Mooij, G. A. Palma, and B. Pradenas, A generalized non-Gaussian consistency relation for single field inflation, *JCAP* **05**, 024 (2018), [arXiv:1711.02680 \[astro-ph.CO\]](#).
  - [109] R. Bravo and G. A. Palma, Unifying attractor and non-attractor models of inflation under a single soft theorem, *Phys. Rev. D* **107**, 043524 (2023), [arXiv:2009.03369 \[hep-th\]](#).
  - [110] G. Ballesteros, J. Rey, M. Taoso, and A. Urbano, Stochastic inflationary dynamics beyond slow-roll and consequences for primordial black hole formation, *JCAP* **08**, 043 (2020), [arXiv:2006.14597 \[astro-ph.CO\]](#).
  - [111] C. Pattison, V. Vennin, D. Wands, and H. Assadullahi, Ultra-slow-roll inflation with quantum diffusion, *JCAP* **04**, 080 (2021), [arXiv:2101.05741 \[astro-ph.CO\]](#).
  - [112] G. Rigopoulos and A. Wilkins, Inflation is always semi-classical: diffusion domination overproduces Primordial Black Holes, *JCAP* **12**, 027 (2021), [arXiv:2107.05317 \[astro-ph.CO\]](#).
  - [113] V. De Luca, G. Franciolini, A. Kehagias, M. Peloso, A. Riotto, and C. Ünal, The Ineludible non-Gaussianity of the Primordial Black Hole Abundance, *JCAP* **07**, 048 (2019), [arXiv:1904.00970 \[astro-ph.CO\]](#).
  - [114] T. Matsubara and M. Sasaki, Non-Gaussianity effects on the primordial black hole abundance for sharply-peaked primordial spectrum, *JCAP* **10**, 094 (2022), [arXiv:2208.02941 \[astro-ph.CO\]](#).
  - [115] G. Franciolini, A. Kehagias, S. Matarrese, and A. Riotto, Primordial Black Holes from Inflation and non-Gaussianity, *JCAP* **03**, 016 (2018), [arXiv:1801.09415 \[astro-ph.CO\]](#).
  - [116] S. Pi and M. Sasaki, Logarithmic Duality of the Curvature Perturbation, *Phys. Rev. Lett.* **131**, 011002 (2023), [arXiv:2211.13932 \[astro-ph.CO\]](#).
  - [117] S. Pi, Non-Gaussianities in primordial black hole formation and induced gravitational waves, (2024), [arXiv:2404.06151 \[astro-ph.CO\]](#).